Eur. Phys. J. D **40**, 423–430 (2006)
DOI: 10.1140/epjd/e2006-00168-1

THE EUROPEAN PHYSICAL JOURNAL D

A semi-dissipative crisis

X.-G. Chao[1,2], J. Dai[1,3], W.-X. Wang[1], and D.-R. He[4,1,a]

[1] College of Physics Science and Technology, Yangzhou University, Yangzhou 225002, P.R. China
[2] Information Science Department, Jiangsu Polytechnic University, Changzhou 213016, P.R. China
[3] College of Mathematics and Physics, Jiangsu University of Science and Technology of China, Zhenjiang 212003, P.R. China
[4] CCAST(World Laboratory), P.O. Box 8730, Beijing 100080, P.R. China

Received 20 July 2005/ Received in final form 27 February 2006
Published online 14 July 2006 –

Abstract. This article reports a sudden chaotic attractor change in a system described by a conservative and dissipative map concatenation. When the driving parameter passes a critical value, the chaotic attractor suddenly loses stability and turns into a transient chaotic web. The iterations spend super-long random jumps in the web, finally falling into several special escaping holes. Once in the holes, they are attracted monotonically to several periodic points. Following Grebogi, Ott, and Yorke, we address such a chaotic attractor change as a crisis. We numerically demonstrate that phase space areas occupied by the web and its complementary set (a fat fractal forbidden net) become the periodic points' "riddled-like" attraction basins. The basin areas are dominated by weaker dissipation called "quasi-dissipation". Small areas, serving as special escape holes, are dominated by classical dissipation and bound by the forbidden region, but only in each periodic point's vicinity. Thus the crisis shows an escape from a riddled-like attraction basin. This feature influences the approximation of the scaling behavior of the crisis's averaged lifetime, which is analytically and numerically determined as $\langle\tau\rangle \propto (b - b_0)^{\gamma}$, where b_0 denotes the control parameter's critical threshold, and $\gamma \simeq -1.5$.

PACS. 05.45.Ac Low-dimensional chaos

1 Introduction

"Crisis", a common manifestation, means sudden chaotic attractor change. Usually the change mechanism is an "escaping hole's" sudden appearance inside a chaotic attractor when a control parameter reaches a threshold value. As the control parameter progresses, the hole gradually grows (from zero measure), so that the motion in the attractor escapes faster. Grebogi, Ott, and Yorke deduced the universal scaling law as

$$\langle\tau\rangle \propto |p - p_c|^{-\gamma}, \tag{1}$$

where $\langle\tau\rangle$ denoted the average iteration lifetime in the original chaotic attractor, p was the system's control parameter, and p_c the control parameter's threshold [1–3]. Grebogi, Ott, and Yorke indicated that in an everywhere smooth dissipative two-dimensional mapping system, the chaotic attractor usually was the unstable manifold closure of a saddle node located in its basin boundary. The stable manifold closure of the same saddle (in a homoclinic case) or another saddle (in a heteroclinic case) formed the chaotic attractor's basin boundary. When the control parameter passed a threshold, the unstable manifold crossed the stable manifold. Consequently, the small region surrounded by the crossing manifolds formed the escaping hole [1–3].

A dissipative system is characterized by continued contraction of phase space volume with increasing time. The well-known reasons for dissipation are friction, heat exchange, etc. Due to these reasons, the trajectories from initial conditions in phase space are attracted monotonically to fixed points, single periodic orbits, or chaotic attractors with lower dimensionality than the original phase space. These attractors often show zero measure in a two-dimensional mapping system. This induces an exponential contraction of phase space volume, a process occurring ad infinitum. However, Wang et al. suggested putting notation on a type of dissipation called "quasi-dissipation" [4,5]. This happens in an irreversible system, in which a phase point might have more than one inverse image, so that some phase space volume elements might "merge to one" in a dynamic process and induce the phase space collapse. The quasi-dissipative mechanism usually leads to a linear collapse of phase space volume. In correspondence, this caused initial values in a phase space area to iterate into elliptical islands with finite measure after a finite period [4–8]. Therefore, quasi-dissipation was always weak relative to well-known classical dissipation. That is

[a] e-mail: darendo10@yahoo.com.cn

why the influence of quasi-dissipation on dynamics usually could not be observed. Only (as Wang et al. did) in a system described by a discontinuous and noninvertible concatenation of two conservative maps was the study of dynamic characteristics induced by quasi-dissipative properties possible, because strong classic dissipation no longer appeared [4–8].

Wang et al. studied crises caused by quasi-dissipative properties and discovered that the crises happened when (one or several) elliptic island(s) suddenly appeared in a chaotic attractor [6–8]. Iterations on the attractor escaped more quickly to the elliptical island when it grew. Jiang et al. studied the lifetime scaling law of the crises in quasi-dissipative systems analytically, and indicated generally that the quasi-dissipative properties did not affect the value of the scaling exponent. Therefore, when estimating, only the "escaping-hole growing rule" and "visiting probability varying rule" [7] were considered. As reported in [6–8], in quasi-dissipative systems, which usually were discontinuous and noninvertible concatenations of two conservative maps, the chaotic attractor always was the image set of the discontinuous borderline in the systemic function's definitional domain. In agreement with the analytic conclusion of Mira in certain kinds of two-dimensional piecewise continuous noninvertible maps (like the system discussed here), the chaotic area was bounded by image segments of the discontinuous borderlines [9].

For an initial condition near a basin boundary, uncertainty in predicting the final attractor can arise because of the finite precision in the initial condition's specification. It may be possible to improve predictability by making the initial condition more precise. If the basin boundary is simple, e.g., a one-dimensional curve in a two-dimensional phase space, increasing the precision will result in an equal amount of improvement in the predictability of the attractor. It has been recognized, however, that in nonlinear dynamical systems significant difficulty can arise in the prediction of the final destination. In particular, fractal basin boundaries [10–12] can arise for which improvement in the precision to specify the initial condition often results in disproportionately less improvement in predictability. Dynamical systems, especially those possessing a simple symmetry, can have riddled basins [13,14], for which vast increase in the precision of the initial condition results in practically no improvement in predictability. Predictability is usually characterized by examining how error probability in the prediction, $f(\epsilon)$, scales with the precision ϵ in the initial condition. Typically, $f(\epsilon) \sim \epsilon^{\alpha}$ where $0 \leq \alpha \leq 1$ is the uncertainty exponent [10]. The value of α determines the degree of improvement in predictability (i.e., decrease in $f(\epsilon)$) upon reduction in ϵ. For fractal basin boundaries, the typical values of α are between zero and unity, while for riddled basins, $\alpha \approx 0$.

Recently, Lai et al. presented a class of nonsymmetrical physical systems that exhibited such an extreme degree of unpredictability in attractors. The system was piecewise smooth Hamiltonian (some example systems were suggested in Refs. [4–8]). Lai et al. discovered that, in the case where multiple attractors coexisted, the attraction basins arisen in such quasi-dissipative systems were mixed in such a way that, for every initial condition that approached one attractor, there were initial conditions arbitrarily nearby that approached other attractors [15]. The mechanism for the unpredictability was found to be different from riddling. It was due to mixing different attraction basins on a fat-fractal set, which was addressed as the "forbidden region net" in references [15,16]. The forbidden region net contained attraction basins of all attractors in the system and the basin boundaries merely divided the fat-fractal sets on all scales. The basins generated by this mechanism were called "riddled-like basins" in reference [15].

This article discusses a system described by a discontinuous and noninvertible concatenation of a conservative and classical dissipative map (addressed as a "semi-dissipative system"). The mechanism (presented by Lai et al. in Ref. [15]) for generating riddled-like basins and total attractor unpredictability can still be observed in this system. The riddled-like basins are dominated by quasi-dissipation and occupy most of the areas in phase space. However, there are small areas dominated by classical dissipation and bound by the forbidden region, but only in each periodic point's vicinity. This can suddenly induce a change of a chaotic attractor into a transient chaotic web, which can be defined as a characteristic crisis (after Grebogi, Ott, and Yorke [1–3]). After the crisis, the iterations on the transient chaotic web (i.e. in the riddled-like basin) escape to certain periodic points. In the second section the system is introduced. In section three the forbidden region is discussed and the affects of classical dissipative or quasi-dissipative properties are explained, respectively. In the fourth section, the characteristic crisis and lifetime scaling law are reported. In the last section, the text is summarized.

2 The semi-dissipative system

The kinds of systems in the current study can be generically described as follows: The system's phase space is divided into two distinct but complementary regions (R_1 and R_2). Such regions are the domains of map functions g_1 and g_2, respectively. The functional forms of g_1 and g_2 are different, therefore the system's dynamics suffer from "jumping" when iterations cross the smooth "discontinuous borderlines" (which divide R_1 and R_2). Additionally, the map composed of g_1 and g_2 shows irreversibility, so that one phase point may have two pre-images. One of the maps, g_1 or g_2, is conservative and the other classically dissipative. As introduced in last section, the systems should show quasi-dissipation and classical dissipation simultaneously. Also, the discontinuous borderlines' forward image set forms a stochastic web where iterations display chaotic motion. The questions are (1) if it is possible to distinguish the different affects of these two types of dissipation on system's dynamics, and (2), if the aforementioned riddled-like attraction basin, induced by coexistence of attractors and the appearance of a fat fractal forbidden net, can still appear. The positive answers to these questions

should lead to interesting dynamic characteristics in such systems.

Such systems basic characteristics should be independent from the details of the mapping functions. Therefore, to answer the questions, a sample system, whose function can be analytically deduced with a model electronic relaxation oscillator (explained in the appendix) can be studied. It is emphasized that the model can be realized with high precision using modern electronic units, and the model is only one of many possible physical backgrounds for the deduction of similar maps. The maps read:

$$\begin{cases} x_{n+1} = g_{1x} = x_n + y_{n+1} + (a/b), \\ y_{n+1} = g_{1y} = y_n - (1/b)\sin(2\pi x_n), \\ \qquad\qquad [\text{mod. } 1] \quad (x_n \notin F), \end{cases} \tag{2}$$

$$\begin{cases} x_{n+1} = g_{2x} = x_n + \frac{\alpha}{2\pi}\ln\dfrac{1+cd}{1-ad-bdy_n}, \\ y_{n+1} = g_{2y} = y_n + 2x_n, \\ \qquad\qquad [\text{mod. } 1] \quad (x_n \in F), \end{cases} \tag{3}$$

where x and y are variables, $F = [x_{F1}, x_{F2}] = [0.5 + \arcsin(c)/(2\pi), 1 - \arcsin(c)/(2\pi)]$ (i.e. the definition region of mapping function g_2), a, b, c, d, α are constants. They satisfy $a > 1$, $b > 0$, $0 < c < 1$, $\alpha > 0$, $0 < d < 1$, respectively. (a, b, c, d are dimensionless and the unit of α is rad).The physical implications of the variables and the constants are explained in appendix.

The Jacobian matrix of maps (2) and (3) are J_1 and J_2, respectively:

$$J_1 = \frac{\partial(x_{n+1}, y_{n+1})}{\partial(x_n, y_n)} = \begin{bmatrix} 1 - \dfrac{2\pi}{b}\cos(2\pi x_n) & 1 \\ -\dfrac{2\pi}{b}\cos(2\pi x_n) & 1 \end{bmatrix} \tag{4}$$

$$J_2 = \frac{\partial(x_{n+1}, y_{n+1})}{\partial(x_n, y_n)} = \begin{bmatrix} 1 & \dfrac{abd}{2\pi(1-ad-bdy_n)} \\ 2 & 1 \end{bmatrix}. \tag{5}$$

The value of the determinant of J_1 is a unit; therefore map (2) is conservative. The value of the determinant of J_2 is less than 1 (within the range of parameters chosen in the current study), therefore map (3) is a classical dissipative map.

The inverse maps of (2) and (3) are:

$$\begin{cases} x_n = g_{1x}^{-1} = x_{n+1} - y_{n+1} - \frac{a}{b}, \\ y_n = g_{1y}^{-1} = y_{n+1} + \dfrac{1}{b}\sin(2\pi x_n), \end{cases} \qquad (x_n \notin F), \tag{6}$$

$$\begin{cases} x_n = g_{2x}^{-1} = (y_{n+1} - y_n)/2, \\ y_n = g_{2y}^{-1} = y_{n+1} - 2x_{n+1} + \dfrac{\alpha}{\pi}\ln\dfrac{1+cd}{1-ad-bdy_n}, \\ \qquad\qquad (x_n \in F). \end{cases} \tag{7}$$

Note that choosing an inverse image is determined by x_n instead of x_{n+1}, therefore each point may have two inverse images, respectively, by (6) or (7). As a result, the concatenation of maps (2) and (3) is irreversible. This induces the quasi-dissipative properties mentioned in the last section. The system is described by a discontinuous and noninvertible concatenation of a conservative and classical dissipative map (a semi-dissipative system).

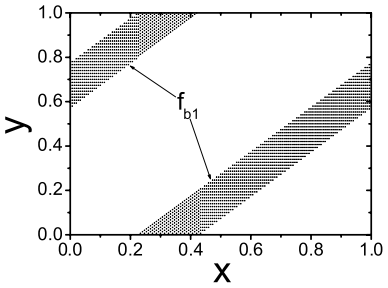

Fig. 1. The f_{b1} region. Parameter values are $\alpha = 1$, $a = 2.0$, $b = 1.27$, $c = 0.8$, $d = 0.09$.

The system's periodic orbits are important to the crisis in the fourth section. The periodic orbits of map (2) have been already discussed in reference [4]. The conclusion that map (3) does not have period-1 orbit can be analytically obtained, but the deduction is trivial and will not be presented. The important periodic orbits are the ones which cross the border, for example, of the period-2 orbit (x_1, y_1), (x_2, y_2), satisfying the following relations:

$$\begin{cases} x_2 = g_{1x}(x_1, y_1) \\ y_2 = g_{1y}(x_1, y_1) \end{cases} \qquad \begin{cases} x_1 = g_{2x}(x_2, y_2) \\ y_1 = g_{2y}(x_2, y_2) \end{cases}. \tag{8}$$

However, it is difficult to analytically deduce their explicit functions. The crisis discussed in the fourth section concerns a period-4 and period-8 orbit. Both cross the border. It is easy to list their implicit expressions similar to (8), but they can be only discussed further by a numerical method (as can be seen in fourth section).

3 The forbidden network

This system is described by a concatenation of a conservative map (2) and a classical dissipative map (3). The definition domains of conservative map g_1 and classical dissipative map g_2 are $D = \{(x, y)|_{0 \le x \le x_{F1} \text{ "or" } x_{F2} \le x \le 1}\}$ and $F = \{(x, y)|_{x \in [x_{F1}, x_{F2}]}\}$, respectively. The forbidden region of map (2), f_{b1}, is defined as the region where every point's backward image $g_1^{-1}(P)$ $P \in f_{b1}$ falls in the definition range of map (3), i.e. $g_1^{-1}(P) \in F$, and thus it does not exist. Similarly, the main part of map (3)'s forbidden region (to be explained in the following paragraph), f_{b2}^1, is defined as the region where every point's backward image $g_2^{-1}(P)$ $P \in f_{b2}^1$ falls in the definition range of map (2), i.e. $g_2^{-1}(P) \in D$, and thus it does not exist.

From inverse map (6) the boundary equation of f_{b1} as $x_{n+1} - a/b + m - x_{F2} \le y_{n+1} \le x_{n+1} - a/b + m - x_{F1}$ can be obtained, where m is an integer denoting the operation of modulo arithmetic. Figure 1 shows f_{b1} region.

Obtaining an explicit expression of region f_{b2}^1 is difficult due to the implicit function form of inverse map (7). It can only be determined by numerical method. The dark gray areas in Figure 2 show region f_{b2}^1. The light gray areas in Figure 2 show the forward image set of the area F denoted by $M = \{(x, y)|_{g_2^{-1}(x,y) \in F}\}$. After the two gray

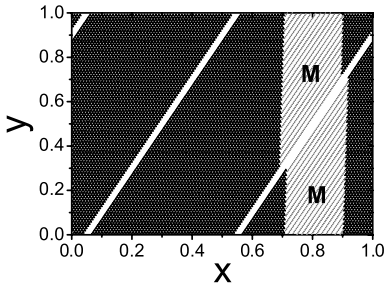

Fig. 2. The f_{b2} region (the dark gray areas and white pinstripes). Parameter values are $\alpha = 1$, $a = 2.0$, $b = 1.27$, $c = 0.8$, $d = 0.09$.

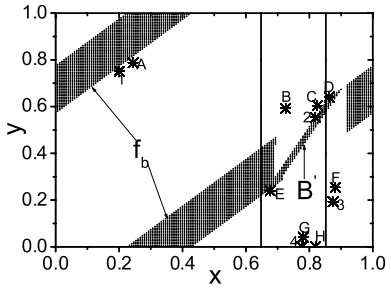

Fig. 3. The phase plane when $\alpha = 1$, $a = 2.0$, $b = 1.27$, $c = 0.8$, $d = 0.09$. It was drawn by selecting evenly 10×10 initial values in area $x \in [0, 1], y \in [0, 1]$, performing 100000 iterations, and recording the last 1000. The nodal points 1, 2, 3, 4 denote a period-4 orbit. The nodal points A, B, C, D, E, F, G, H denote a period-8 orbit. The dark shadowed areas show the forbidden region. B' indicates the forbidden area induced by strong-dissipative properties.

areas are removed, in Figure 2 there are surplus parts denoted by three white, narrow, strap-shaped areas. They show the collapsed part of the phase plane induced by the classical dissipation of map g_2, which can be denoted by $f_{b2}^2 = I - g_2(I)$ (I denotes the whole phase plane $\{(x, y)|_{x\in[0,1],y\in[0,1]}\}$). Obviously, because the iteration of the whole phase plane by g_2 falls out of f_{b2}^2, f_{b2}^2 is also a part of map (3)'s forbidden region, f_{b2}, which means $f_{b2} = f_{b2}^1 \cup f_{b2}^2$.

The system's forbidden region, where the iterations starting from any other place in the phase plane cannot enter, is defined as $f_b = f_{b1} \cap f_{b2}$. The forward images of f_b seem also to be the forbidden region, however, some points there may have two backward images. One of them belongs to the forbidden region; the other is outside of it. Therefore the real forbidden region should be the forward image set of f_b, excluding the points which have two backward images. It can be expressed as $F_r = \bigcup_{j=1}^{\infty}[g^j(f_b)\backslash Q]$, where Q denotes the set of points which have two backward images. Obviously, F_r should be a fat fractal network [15,16]. The boundaries of the forbidden network, F_r, should be the forward images of the discontinuous borderlines [15,16]. The forbidden network and the stochastic web formed by the forward image set of the discontinuous borderlines are complementary on phase space [15,16]. Trajectories initiated from the forbidden net must exit immediately and, once exiting, can no longer return to the set. The next section shows that the forbidden network plays an important role on the crisis discussed in the section.

The gray areas in Figure 3 show forbidden region f_b, where the narrow stripe-shaped part denoted by B' shows the forbidden area induced by classical dissipative properties. The numerical calculation indicates that the area of B' just equals the area of collapse caused by the iteration of area F, by g_2. The next section introduces B''s important role in a characteristic crisis.

4 The crisis

A crisis is observed in the current system where classical dissipation and quasi-dissipation coexist. However, as it is possible to distinguish their different affects, the crisis shows special features. In the current study, the parameters in maps (2) and (3) are chosen as $a = 2.0$, $c = 0.8$, $d = 0.09$, and $\alpha = 1$ (rad), and b is chosen as the control parameter.

When the control parameter decreases and reaches $b = 1.400$, a period-4 point attractor, which crosses the border, appears and coexists with elliptic islands. This means a new phenomenon that is coexistent with elliptic islands and point attractors (periodic orbits) emerges. When the control parameter decreases further and reaches $b = 1.356$, all the elliptic islands disappear nearly simultaneously due to collision with the discontinuous borderline. When the control parameter decreases further and reaches $b = 1.278$, a period-8 point attractor, which also crosses the border, appears and coexists with the period-4 point orbit as shown in Figure 3. When $b = b_0 = 1.2691$, the "key attracting point" (denoted by "2" in Figure 3, located at $x_g = 0.81948, y_g = 0.55597$) collides with the boundary of the forbidden area B'. The period-8 point attractor disappears at almost the same time due to the same reason. A chaotic attractor then dominates the phase plane.

When the control parameter increases from $b_0 = 1.2691$, the chaotic attractor suddenly loses stability and turns into a transient chaotic web as shown in Figure 4a (at $b = 1.2707$) by black points (it resembles the chaotic attractor existing at $b < b_0 = 1.2691$ very well and is the image set of the discontinuous borderline as discussed in the first and third sections. The black points are drawn when $b = 1.2707$, by evenly selecting 10×10 initial values and then recording 1000 iterations from each value after ignoring the first 1000). All the iterations on the transient chaotic web approach period-4 and period-8 point attractors. The chaotic attractor's sudden change is defined as a crisis [1–3].

The dark gray (green online) areas in Figure 4a (at $b = 1.2707$) show the forbidden region stated in the last section. The small brighter gray (dark yellow online) areas show the first image. The remaining part of the forbidden fat fractal network, F_r, is shown by the white areas. The small black spots denote the transient chaotic web as stated in last paragraph. The two black (blue online)

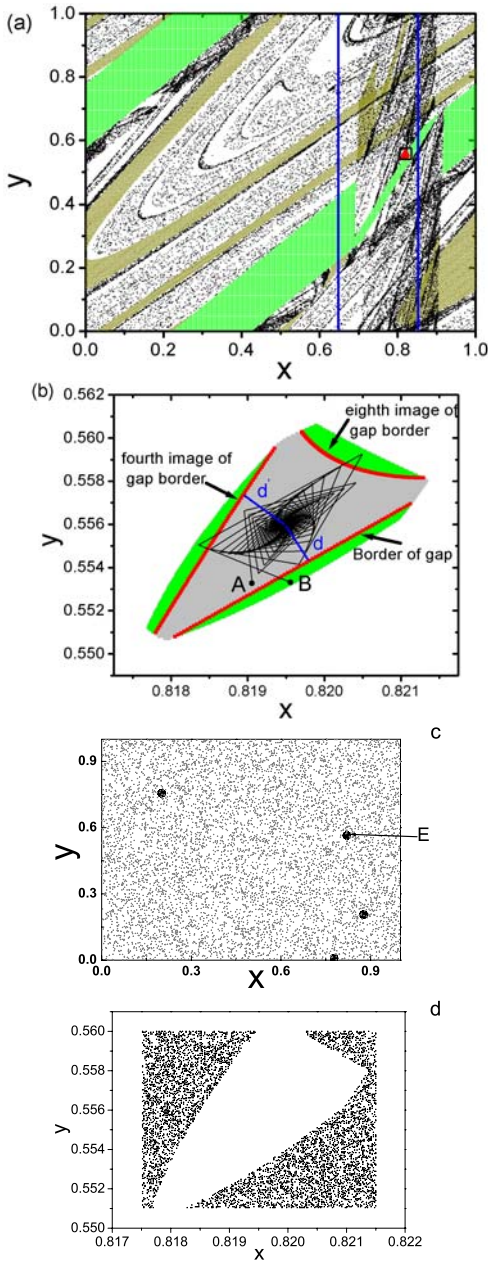

Fig. 4. (Color online) (a) The phase plane at $b = 1.2707$; (b) magnification of the (red online) rectangular region shown in (a); (c) the attraction basins of period-4 and -8 point attractors at $b = 1.2707$; (d) magnification of the area E in (c).

vertical lines denote the discontinuous borderlines. The small black (red online) rectangular area is magnified (as shown in Fig. 4b (at $b = 1.2707$)), where a triangular area is shown by dark gray (green on line) and lighter gray colors separated by three black (red online) lines. The thin black solid lines starting from initial points A or B, respectively, show that all the iterations starting from a point inside the triangle never leave the area, and approach the key period-4 point located at the center.

Figure 4c shows the numerical results about the attraction basins of the two periodic (period-4 and -8) attractors. The gray areas show the initial values attracted to the period-8 point attractor, while the white areas show the initial values attracted to the period-4 point attractor (they are drawn by selecting evenly 1000×1000 initial values in $x \in [0,1], y \in [0,1]$, then showing an initial value in white if the iterations from it reach $|x - x_g| \leq 0.000001, |y - y_g| \leq 0.000001$ inside 500000 iterations. The criterion for approaching period-8 is similar and will not be repeated). This figure shows that the basins are riddled-like. The riddled-like attraction basin was believed to be a common feature of systems described by a discontinuous and noninvertible concatenation of two conservative maps due to the fact that the fat fractal forbidden network contains attraction basins of all attractors in the system, and the basin boundaries merely divide the fat-fractal sets on all scales [15]. The example shows that the phenomenon also appears in systems described by a discontinuous and noninvertible concatenation of a conservative and a classical dissipative map. This conclusion is reasonable because the fat fractal forbidden network still appears in the current system as discussed in the last section.

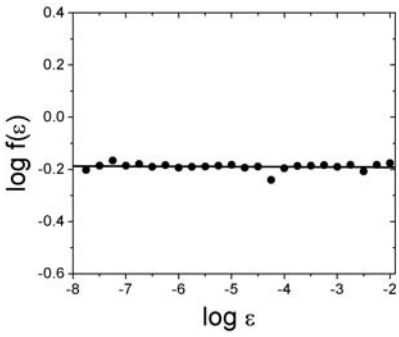

Fig. 5. The numerically obtained $f(\epsilon) - \epsilon$ relation, $b = 1.2707$.

As described in the first section, the error probability in the prediction of the final attractor for an initial condition, $f(\epsilon)$, scales with the precision ϵ in the initial condition. One typically has $f(\epsilon) \sim \epsilon^{\alpha}$ where the uncertainty exponent $\alpha \approx 0$ for riddled-like basins [10,15]. To verify if this conclusion is common also in systems described by a discontinuous and noninvertible concatenation of a conservative and a classical dissipative map (as reported here), the variation relation of $f(\epsilon) - \epsilon$ has been computed in the following way. We selected evenly 400 initial values in $x \in [0.2, 0.4], y \in [0.2, 0.4]$, and also 400 initial values as $(x + \epsilon, y + \epsilon)$, then computed the proportion, by which the initial values (x, y) and $(x + \epsilon, y + \epsilon)$ approach different point attractors (the period-4 or period-8 orbit), as an approximation of $f(\epsilon)$. The results showing the obtained $f(\epsilon) - \epsilon$ relation are presented in Figure 5, which shows that $f(\epsilon)$ basically does not change when ϵ varies and passes 6 magnitudes. This denotes that the prediction is totally impossible.

Comparing Figures 4a and 4c, one sees that riddled-like basins of the period-4 and period-8 orbits occupy almost all the phase space where the fat fractal forbidden net and transient stochastic web appear. The numerical computation shows proofs for the fact that quasi-dissipation dominates this phase region where iterations

jump randomly and cannot approach a point attractor monotonically. However, Figure 4c also shows extant some small phase space areas with smooth boundaries around each periodic point, where only classical dissipation dominates. The areas around the four period-4 points are shown by four black spots in the figure. The area around the key periodic point, (x_g, y_g), is indicated by "E" and is magnified. Figure 4d shows the magnification where the approximate triangular area is clearly shown, identical to Figure 4b, indicating that the triangular area shown by dark gray (green online) and gray colors in Figure 4b is the smooth boundary attraction basin of the key period-4 point. The crisis is signified by an escape from the quasi-dissipation dominated, riddled-like basin, which occupies almost all the phase space, to the small areas dominated by classical dissipation in the vicinity of periodic points.

However, the area shown by dark gray (green online) and gray colors in Figure 4b is not yet the escaping hole, Δ, of the crisis. Δ must be confined by the forbidden region or its images, since no iterations from other areas can enter these regions. The black (red online) curve at the bottom-right of Figure 4b shows the upper borderline of the forbidden region induced by classical dissipation, B'. The other two black (red online) curves at the top-left or top-right in Figure 4b show the borderlines of the fourth or eighth image of the forbidden region induced by strong dissipation, B'. Therefore only the gray area confined by these three black (red online) curves is the escaping hole, Δ. The numerical result confirms that the fourth and eighth images of the forbidden region induced by classical dissipation, B', move far away as the control parameter b increases, so that the escaping hole Δ becomes increasingly larger, and the average lifetime of the iterations on the transient chaotic web becomes increasingly shorter. Such an escaping hole, which is produced by a small area dominated by classical dissipation inside a very large, riddled-like attraction basin, and also confined by border images of the forbidden region induced by classical dissipation, has never been reported. This is the significant feature of the crisis.

It is now clear that a fat fractal forbidden network exists after the crisis occurs. Trajectories initiated from the network must exit, and once exiting, they can no longer return to the set. Once trajectories leave, they wander (for a very long time) in the transient chaotic web formed by the images of discontinuous borderlines. Since the forbidden region network is a fat-fractal set, points in the network go to different attractors, period-4 orbits, or period-8 orbits, no matter how close the points are. This gives rise to the riddled-like structure observed in numerical experiments. All these phenomena are connected with quasi-dissipative property (the numerical results show that only quasi-dissipation plays a role in the riddled-like attraction basin area); the only expressions of classical dissipation are the escaping holes. In such circumstances, as reference [7] points out, the value of the scaling exponent in the lifetime scaling law, (1), can only be estimated by considering the rule of escaping hole growth and the varying rule of

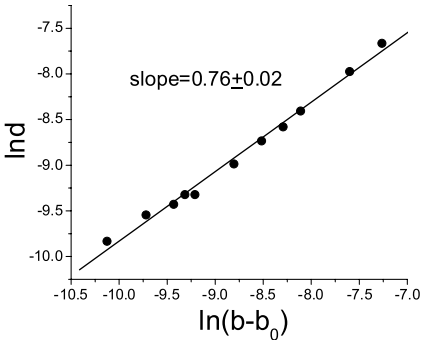

Fig. 6. The variation rule of distance d.

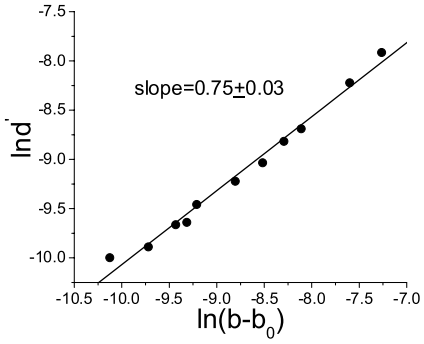

Fig. 7. The variation rule of distance d'.

visiting probability to unit area of escaping hole, i.e.

$$\langle \tau \rangle \propto \frac{1}{\rho \Delta}, \tag{9}$$

where Δ denotes the measure (area) of the aforementioned escaping hole, and ρ denotes visiting probability to unit area of the escaping hole. Due to interest only in the value of the scaling exponent, the escaping hole is considered an approximate triangle. The variation rule of its area can be approximated by the multiplication of d and d', which are distances from the key periodic point to the top-left and bottom-right black (red online) borderlines, as denoted by two black (blue online) linear lines in Figure 4b. Numerically, the variation rules of d and d' are obtained when the control parameter b changes (as shown by Figs. 6 and 7):

$$d \propto (b - b_0)^{0.76 \pm 0.02}, \tag{10}$$

$$d' \propto (b - b_0)^{0.75 \pm 0.02}, \tag{11}$$

which show a variation rule of the escaping hole measure as:

$$\Delta \propto (b - b_0)^{0.75+0.76}. \tag{12}$$

The numerical investigation also confirms that ρ is a constant, independent from control parameter b; therefore, at once the scaling law of the crisis is estimated as:

$$\langle \tau \rangle \propto \frac{1}{\rho \Delta} \propto (b - b_0)^{\gamma}, \tag{13}$$

where $\gamma \simeq -1.51$.

Figure 8 shows the scaling behavior of the average lifetime computed totally in a numerical way. The average

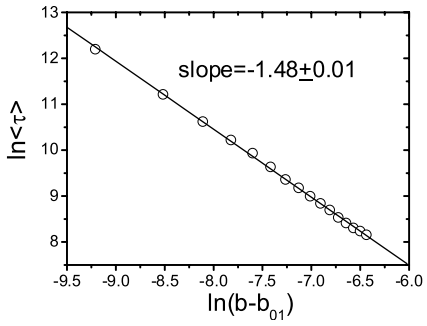

Fig. 8. The scaling behavior of the average lifetime, $\langle\tau\rangle$, in transient chaos. It is computed by evenly selecting 100×100 initial values. The variation range of the control parameter b is between 1.2692 and 1.2707. When $b = 1.2708$, a new period-7 attractor appears, so that the scaling behavior suddenly changes. That is why this variation range is chosen.

lifetime, $\langle\tau\rangle$, is defined as:

$$\langle\tau\rangle = \lim_{n\to\infty} \frac{\sum_{i=1}^{n} N_i}{n}, \tag{14}$$

where n denotes the number of initial values, and N_i denotes the iteration lifetime starting from the initial value i. From the excellent linear fitting on the double-logarithmic plane shown in Figure 8, it is definite that the lifetime scaling in the crisis follows

$$\langle\tau\rangle \propto (b - b_0)^{\gamma}, \tag{15}$$

where $\gamma = -1.48 \pm 0.01$. This is in strong agreement with the above mentioned analysis.

5 Conclusion

A system described by a discontinuous and noninvertible concatenation of a conservative and classical dissipative map is presented. There coexist quasi-dissipation, which expresses its affection widely, and classical dissipation, which shows affection on the system's dynamics only in some phase space regions. This kind of system may display special dynamic phenomena, such as the crisis presented. The most significant feature of the crisis lies in its escaping hole, which is formed by several very small attraction basins with regular boundaries, dominated by classical dissipation, of the periodic points. Most places on the phase plane are occupied by riddled-like attraction basins of different periodic orbits, which give rise to motion in a transient chaotic network formed by image sets of the discontinuous borderline in the system's definition domain.

This investigation pointed out that the significant dynamic features observed only in the systems described by discontinuous and noninvertible concatenations of two conservative maps also belong to systems described by discontinuous and noninvertible concatenations of conservative and classical dissipative maps. The features include the stochastic web formed by forward images of the discontinuous borderlines, the quasi-dissipation property, the riddled-like attraction basin of coexisting attractors, and the fat fractal forbidden network. However, the systems described by discontinuous and noninvertible concatenations of conservative and classical dissipative maps show unique behavior, which the systems described by discontinuous and noninvertible concatenations of two conservative maps cannot show. For example, the classical dissipation and quasi-dissipation show their different and distinguishable effects on the crisis presented here.

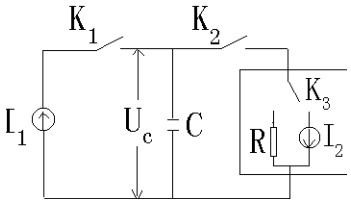

Fig. 9. Schematic of the relaxation oscillator with over-voltage protection and a dissipative unit.

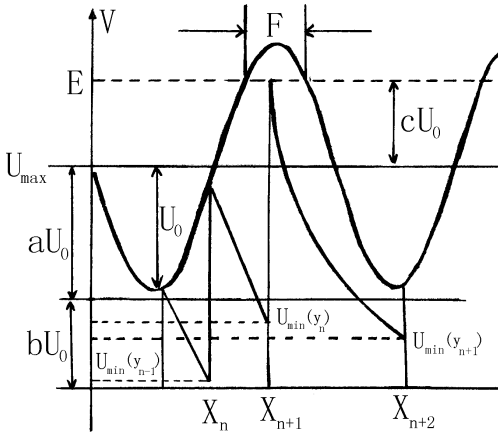

Fig. 10. The relaxation oscillation.

This study was supported by the National Natural Science Foundation of China under Grant No. 10275053. The manuscript was partly written in the Department of Computational Science, National University of Singapore. The corresponding author of this paper wants to express his gratitude to Prof. K. Chen for providing advanced research facilities and valuable financial support from grant R-151-000-032-112.

Appendix: The deduction of map (2) and (3)

The sample system in the current study is similar to the model discussed by Wang et al. in literature [4]. Figure 9 shows its schematic, in which I_1 and I_2 are current sources, K_1, K_2, and K_3 are controllable electronic switches, and $I_1 \gg I_2$. When K_1 switches on and K_2 switches off, I_1 charges the capacitance C extremely fast as Figure 10 shows. When voltage U_c, across the capacitance, rises to an upper threshold value modulated by a sinusoidal signal, and is not larger than a constant E, K_1 switches off and K_2 switches on. In this case K_3 connects I_2, which makes capacitance C discharge slowly through current source I_2.

If U_c is larger than the constant E, K_3 connects resistance R when U_c is just larger than constant E, which makes capacitance C discharge slowly through resistance R. In any case, when U_c falls to a lower threshold value, K_1 switches on and K_2 switches off, then capacitance C turns into the charging state from the discharging state. The lower threshold is modulated by the phase of upper threshold at which the last U_c suddenly falls. The phase point is denoted by a variable x. The modulation function is described by another variable y, which will be explained later. In this way, the circuit oscillates continuously.

Figure 10 shows the relaxation oscillation of U_c and the variation of upper and lower thresholds. As the figure shows, the upper threshold can be expressed as

$$\begin{cases} U_n = U_{max} + U_0 \sin(2\pi x_n), & \\ U_n = U_{max} + cU_0, & \text{when} \quad (x_n \notin F), \\ & \quad (x_n \in F), \end{cases} \tag{16}$$

where U_n denotes upper threshold value when the capacitance suddenly turns from charging to discharging at nth time, x_n denotes the sinusoidal modulation signal phase of upper threshold at the time, U_{max} and U_0 are constants, $F = [x_{F1}, x_{F2}] = [0.5 + \arcsin(c)/(2\pi), 1 - \arcsin(c)/(2\pi)]$ (i.e. the definition region where voltage protection is implemented, which makes U_c suddenly begin falling from constant E), and parameter c satisfies $0 < c < 1$. At the same time, as Figure 10 shows, the lower threshold is modulated by phase x_n with the relation:

$$U_{min}(y_n) = U_{max} - aU_0 - by_nU_0, \tag{17}$$

$$\begin{cases} y_{n+1} = y_n - (1/b)\sin(2\pi x_n), & \\ y_{n+1} = y_n + (4\pi)/(bU_0), & \text{when} \quad (x_n \notin F), \\ & \quad (x_n \in F), \end{cases} \tag{18}$$

where parameters a and b satisfy $a > 1$ and $b > 0$, respectively. Figure 10 illustrates that the lower threshold is confined between $U_{max} - aU_0$ and $U_{max} - aU_0 - bU_0$, and $y_n \in [0, 1]$. When $y_n = 0$, $U_{min} = U_{max} - aU_0$; when $y_n = 1$, $U_{min} = U_{max} - aU_0 - bU_0$.

The following relation is obtained:

$$C[U_c(x_n) - U_{min}(y_n)] = I_2 \frac{2\pi(x_{n+1} - x_n)}{\omega}, \tag{19}$$

where ω is the modulation signal frequency of the upper threshold. When $x_n \notin F$, it is assumed that $C\omega/I_2 = 1$, $bU_0/2\pi = 1$ (the units of both quantities are rad/V, V, respectively), and map (2) can be obtained.

When $x_n \in F$, the capacitance discharges though the resistance R. From $dQ = CdU_c$ one can obtain $-dt = [(RC)/U_c]dU_c$. Integrating the equation for the discharge process $t_n \to t_{n+1}$, one reaches $-(t_{n+1} - t_n) = RC[\ln U_c(t_{n+1}) - \ln U_c(t_n)]$. Putting $U_c(t_{n+1}) = U_{min}(y_n) = U_{max} - aU_0 - by_nU_0$, $U_c(t_n) = U_n^{up} = U_{max} + cU_0$ into the above equation, and noting that $t_{n+1} - t_n = 2\pi(x_{n+1} - x_n)/\omega$, one gets

$$x_{n+1} - x_n = \frac{RC\omega}{2\pi} \ln \frac{U_{max} + cU_0}{U_{max} - aU_0 - by_nU_0}.$$

Let $RC\omega = \alpha$ (the unit of α is rad), one gets

$$x_{n+1} - x_n = \frac{\alpha}{2\pi} \ln \frac{U_{max} + cU_0}{U_{max} - aU_0 - by_nU_0}.$$

Let $d = U_0/U_{max}$, and one reaches

$$x_{n+1} = x_n + \frac{\alpha}{2\pi} \ln \frac{1 + cd}{1 - ad - bdy_n}.$$

Consider $y_{n+1} = y_n + (4\pi/bU_0)x_n$ and note $bU_0/2\pi = 1$, equation (3) is obtained.

References

1. C. Grebogi, E. Ott, J.A. Yorke, Phys. Rev. Lett. **48**, 1507 (1982); C. Grebogi, E. Ott, J.A. Yorke, Physica D **7**, 181 (1983)
2. C. Grebogi, E. Ott, J.A. Yorke, Phys. Rev. Lett. **57**, 1284 (1986); C. Grebogi, E. Ott, J.A. Yorke, Phys. Rev. A **36**, 5365 (1987)
3. C. Grebogi, E. Ott, J.A. Yorke, Phys. Rev. Lett. **50**, 935 (1983); C. Grebogi, E. Ott, J.A. Yorke, Ergod. Theor. Dynam. Sys. **5**, 341 (1985)
4. J. Wang, X.L. Ding, B. Hu, B.H. Wang, J.S. Mao, D.R. He, Phys. Rev. E **64**, 026202 (2001)
5. J. Wang, X.L. Ding, B.H. Wang, D.R. He, Chin. Phys. Lett. **18**, 13 (2001)
6. X.M. Wang et al., Eur. Phys. J. D **19**, 119 (2002)
7. Y.M. Jiang, Y.Q. Lu, X.G. Chao, D.R. He, Eur. Phys. J. D **29**, 285 (2004)
8. Y. He, Y.M. Jiang, Y. Shen, D.-R. He, Phys. Rev. E **70**, 056213 (2004)
9. C. Mira, Inter. J. Bifur. Chaos **6**, 893 (1996)
10. C. Grebogi, S.W. McDonald, E. Ott, J.A. Yorke, Phys. Lett. A **99**, 415 (1983); S.W. McDonald, C. Grebogi, E. Ott, J.A. Yorke, Physica D **17**, 125 (1985)
11. F.T. Arecchi, R. Badii, A. Politi, Phys. Rev. A **29**, 1006 (1984); F.T. Arecchi, A. Califano, Phys. Lett. A **101**, 443 (1986)
12. F.C. Moon, Phys. Rev. Lett. **53**, 962 (1984); F.C. Moon, G.-X. Li, Phys. Rev. Lett. **55**, 1439 (1985); E.G. Gwinn, R.M. Westervelt, Phys. Rev. A **33**, 4143 (1986)
13. J.C. Alexander, J.A. Yorke, Z. You, I. Kan, Int. J. Bifur. Chaos **2**, 795 (1992); E. Ott, J.C. Alexander, I. Kan, J.C. Sommerer, J.A. Yorke, Physica D **76**, 384 (1994); P. Ashwin, J. Buescu, I.N. Stewart, Phys. Lett. A **193**, 126 (1994); P. Ashwin, J. Buescu, I.N. Stewart, Nonlinearity **9**, 703 (1996); J.F. Heagy, T.L. Carroll, L.M. Pecora, Phys. Rev. Lett. **73**, 3528 (1994); Y.-C. Lai, C. Grebogi, Phys. Rev. E **52**, R3313 (1995); H. Nakajima, Y. Ueda, Physica D **99**, 35 (1996); L. Billings, J.H. Curry, E. Phipps, Phys. Rev. Lett. **79**, 1018 (1997); K. Kaneko, Phys. Rev. Lett. **78**, 2736 (1997); Y.L. Maistrenko, V.L. Maistrenko, A. Popovich, E. Mosekilde, Phys. Rev. E **57**, 2713 (1998); T. Kapitaniak, Y. Maistrenko, A. Stefanski, J. Brindley, Phys. Rev. E **57**, R6253 (1998); M. Woltering, M. Markus, Phys. Rev. Lett. **84**, 630 (2000)
14. Y.-C. Lai, C. Grebogi, J.A. Yorke, S.C. Venkataramani, Phys. Rev. Lett. **77**, 55 (1996)
15. Y.C. Lai, D.-R. He, Y.M. Jiang, Phys. Rev. E **72**, 025201(R) (2005)
16. J. Dai, W.X. Wang, Y.M. Jiang, Y. He, W. Chen, D.-R. He, Chin. Phys. Lett. **22**, 827 (2005); J. Dai, W.X. Wang, Y.M. Jiang, Y. He, W. Chen, D.-R. He, Chin. Phys. **14**, 1334 (2005)